International Journal of Nanomedicine

Dovepress
open access to scientific and medical research

Open Access Full Text Article

ORIGINAL RESEARCH

Combining Olaparib and Ascorbic Acid on Nanoparticles to Enhance the Drug Toxic Effects in Pancreatic Cancer

Francisco Quiñonero[1,2,*], Belén Parra-Torrejón[3,*], Gloria B Ramírez-Rodríguez[3], Victor Garcés[3], José M Delgado-López[3], Cristina Jiménez-Luna[1,2,4], Gloria Perazzoli[1,2,4], Consolación Melguizo[1,2,4], Jose Prados[1,2,4], Raul Ortíz[1,2,4]

[1]Institute of Biopathology and Regenerative Medicine (IBIMER), Center of Biomedical Research (CIBM), University of Granada, Granada, 18100, Spain; [2]Instituto de Investigación Biosanitaria de Granada (ibs.GRANADA), Granada, 18014, Spain; [3]Department of Inorganic Chemistry, Faculty of Science, University of Granada, Granada, 18071, Spain; [4]Department of Anatomy and Embryology, Faculty of Medicine, University of Granada, Granada, 18071, Spain

*These authors contributed equally to this work

Correspondence: José M Delgado-López, Department of Inorganic Chemistry, Faculty of Science, University of Granada, Granada, 18071, Spain, Email jmdl@ugr.es

Introduction: Pancreatic cancer (PC) shows a very poor response to current treatments. Development of drug resistance is one of the causes of the therapy failure, being PARP1 (poly ADP-ribose polymerase 1) a relevant protein in the resistance mechanism. In this work, we have functionalized calcium phosphate-based nanoparticles (NPs) with Olaparib (OLA, a PARP-1 inhibitor) in combination with ascorbic acid (AA), a pro-oxidative agent, to enhance their individual effects.

Methods: Amorphous Calcium Phosphate (ACP) NPs were synthesized through a biomimetic approach and then functionalized with OLA and AA (NP-ACP-OLA-AA). After evaluation of the loading capacity and release kinetic, cytotoxicity, cell migration, immunofluorescence, and gene expression assays were performed using pancreatic tumor cell lines. In vivo studies were carried out on tumors derived from the PANC-1 line in NOD SCID gamma (NSG) mice.

Results: NP-ACP-OLA-AA was loaded with 13%wt of OLA (75% loading efficiency) and 1% of AA, respectively. The resulting dual nanosystem exhibited a gradual release of OLA and AA, being the latter protected from degradation in solution. This ensured the simultaneous availability of OLA and AA for a longer period, at least, during the entire time of in vitro cell experiments (72 hours). In vitro studies indicated that NP-ACP-OLA-AA showed the best cytotoxic effect outperforming that of the free OLA and a higher genotoxicity and apoptosis-mediated cytotoxic effect in human pancreatic ductal adenocarcinoma cell line. Interestingly, the in vivo assays using immunosuppressed mice with PANC-1-induced tumors revealed that NP-ACP-OLA-AA produced a higher tumor volume reduction (59.1%) compared to free OLA (28.3%) and increased the mice survival.

Conclusion: Calcium phosphate NPs, a highly biocompatible and biodegradable system, were an ideal vector for the OLA and AA co-treatment in PC, inducing significant therapeutic benefits relative to free OLA, including cytotoxicity, induction of apoptosis, inhibition of cell migration, tumor growth, and survival.

Keywords: nanomedicine, calcium phosphate nanocarriers, Olaparib, ascorbic acid, synergistic effect, pancreatic cancer

Introduction

Pancreatic cancer (PC) is one of the major causes of cancer deaths. Between 80% and 85% of patients are diagnosed in a too advanced stage, which prevents the tumor resection. Even so, when resection occurs, the survival rate of patients is usually relatively low (about 20% at 5 years).[1] Also, there is an absence of effective chemotherapeutic agents when the tumor is irresectable. Among them, Gemcitabine has been the agent of choice since the 1990s, but better response rates have been observed using FOLFIRINOX, a combination of different drugs (5-fluorouracil, leucovorin, irinotecan, and oxaliplatin). Furthermore, co-treatment of nab-Paclitaxel with Gemcitabine had increased the half-life compared to the use of Gemcitabine

Received: 24 April 2023
Accepted: 29 June 2023
Published: 6 September 2023

Graphical Abstract

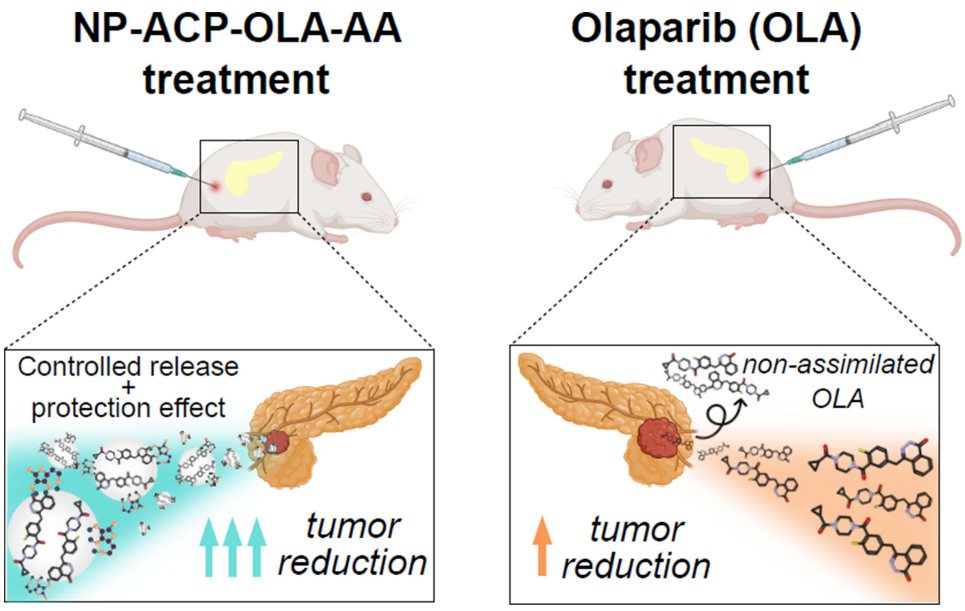

alone. The low survival rate requires new and more effective treatments to improve the patient's quality of life.[2,3] In recent years, Poly ADP-ribose polymerase (PARP) inhibitors have shown efficacy in breast and ovarian cancer cells that possess depletions in DNA repair genes, especially in breast cancer (BRCA).[4] The PARP family inhibition effect is caused due to its important role in the repair of DNA damage in a non-homologous pathway (NHEJ) and in homologous recombination (HR) through the modification of proteins with ADP-ribose residues that allow the formation of repair complexes of DNA in a more efficient way.[5] Available PARP inhibitors include OLA, Rucaparib, Veliparib, Niraparib, Talazoparib, and Pamiparib, being OLA the most extended. A clinical trial determined the efficacy of Olaparib (OLA) as maintenance therapy in patients with BRCA-mutated metastatic tumors.[6] However, OLA therapy has serious drawbacks including limited bioavailability, poor plasma stability (rapid plasma clearance rate), low tissue perfusion, inefficient cellular uptake, and drug resistance. Thus, relatively large amounts of drug must be administered exceeding dose-limiting normal tissue toxicity.[7,8]

The combination of chemotherapeutic agents holds great promise to overcome these limitations. The synergistic effects caused by the co-administration of multiple therapeutic agents against tumor cells lead to elevated tumor inhibition efficiency, enhanced sensitivity of tumors to therapeutic agents, and decreased adverse effects.[9] The combination of OLA and a selective agent for damaging tumoral DNA such as ascorbic acid (AA) may benefit PC patients with BRCA mutations.[10] AA generates reactive oxygen species (ROS) as hydrogen peroxide (H_2O_2), which alter redox-active labile iron metabolism in cancer cells, whereas in healthy cells these species are promptly metabolized.[11] Thus, AA could be an appropriated and selective agent for damaging tumoral DNA, enhancing OLA effectiveness.[10] Despite the great promise of this combination strategy for clinical application, the simultaneous co-delivery at optimal ratio at tumor sites is still a great challenge due to the completely different pharmacokinetic behaviors of each drug. The use of nanotechnology has provided new opportunities for the controlled and synchronized co-delivery of specific cargoes intracellularly, improving their bioavailability, decreasing the dose, and reducing the side effects on healthy cells.[9] Engineered nanoparticles (NPs) have the potential to improve the stability and solubility of encapsulated cargos, promote transport across membranes, and prolong circulation times to increase safety and efficacy.[12] The encapsulation of cisplatin and OLA into layer-by-layer liposomal nanoparticles provided prolonged blood circulation half-life, mechanistic staged drug release and targeted codelivery of the therapeutic agents to high-grade serous ovarian cancer.[7] This treatment resulted in significantly reduced tumor metastasis, extended survival, and moderated systemic toxicity in mice in comparison to the

free drugs. Tumor-targeting nano-drug system for the co-delivery of OLA and adavosertib (WEE1 inhibitors) enhanced the antitumor effect on ovarian cancer while minimizing undesired toxic side effects of free drug administration.[13] The co-delivery of OLA and gemcitabine from peptide nanoparticles significantly suppressed tumor growth in a murine pancreatic cancer model while minimizing side effects.[8]

Synthetic calcium phosphate NPs similar to those found in bone, either apatite (Ap) or amorphous calcium phosphate (ACP), are well-established biomaterials, especially in orthopaedic and trauma surgery due to their outstanding biocompatibility, bioactivity, and biodegradability.[14] Moreover, they have been successfully used in nanomedicine for the controlled delivery of different therapeutic agents (*eg*, chemotherapeutic drugs, antibiotics, growth factors, proteins, antibodies, RNA, and DNA) thanks to their ability to bind a wide variety of molecules due to their large surface area-to-volume ratio.[15] Degradability of the calcium phosphate NPs in acidic tumor microenvironment or endolysosomal organelles due to their pH-dependent solubility is the other major characteristic which makes them favorable candidates towards their clinical translational applications.[16] Recently, calcium-containing nanosystems have been regarded as oncological drug alternatives since the imbalance in calcium homeostatic supported by ROS agents has consequences in cancer.[17] Actually, Chen et al have demonstrated an improvement in pancreatic cancer therapy due to the synergistic effect between the chemotherapeutic 5-fluorouracil (5-Fu) and Ca^{2+} from calcium phosphate nanocarriers.[18]

Considering those precedents, calcium phosphate NPs can be considered as a biocompatible nanoplatform able to simultaneously deliver OLA and AA upon NP dissolution, enhancing the drug-associated antitumoral effects. This work is indeed aimed at developing innovative dual nanoplatforms containing OLA and AA for the effective treatment of PC. The calcium phosphate-based nanoplatforms have been in-depth characterized, and the simultaneous release of the two molecules was evaluated. The effectiveness of the dual nanosystem in comparison to free OLA (alone or combined with AA) has been demonstrated in in vitro and in vivo, where antiproliferative effect and mice survival were more favorable evidencing the combinatory effects of our nanosystems.

Materials and Methods

Materials

Sodium citrate tribasic dihydrate ($Na_3(C_6H_5O_7)\cdot 2H_2O$, ≥99.0% pure), potassium phosphate dibasic anhydrous (K_2HPO_4, ≥99.0% pure), sodium carbonate (Na_2CO_3 ≥99.0% pure), calcium chloride dihydrate ($CaCl_2\cdot 2H_2O$ ≥99.0% pure), ascorbic acid ($C_6H_8O_6$ ≥99.0% pure), and Sodium Hydroxide (NaOH ≥99.0%, pellets for analysis) were purchased from Sigma-Aldrich. OLA ($C_{24}H_{23}FN_4O_3$ ≥99.0% pure, powder) was purchased from MedChemExpress. Anhydrous dimethyl sulfoxide (DMSO) ($(CH_3)_2SO$ ≥99.0%) was employed to dissolve OLA. All the solutions were prepared in ultrapure water (0.22μS, 25°C, Milli-Q, Millipore) and sterile conditions.

Synthesis and Functionalization of the Nanoparticles

Amorphous calcium phosphate nanoparticles (NP-ACP) were synthesized by a so-called biomimetic approach, in the presence of carbonate and citrate ions, with the aim of mimicking the composition of bone NPs.[19] Briefly, two solutions (A) $CaCl_2$ (0.2 M) and Na_3Cit (0.2 M) and (B) K_2HPO_4 (0.12 M) and Na_2CO_3 (0.1 M) were mixed (1:1 v/v 200 mL total) and stirring for 5 minutes. NP-ACP were collected and washed twice with ultrapure water via centrifugation (6000 rpm, 15 minutes, 10° C). Then, the NPs were functionalized with OLA (NP-ACP-OLA). The optimal conditions were obtained by adding 1 g of NPs in 16 mL of water containing 132 mg of OLA (previously dissolved in DMSO). The mixture was stirred for 24h at room temperature and subsequently, NP-ACP-OLA were collected by centrifugation (12,500 rpm, 2 minutes, 10° C).

NP-ACP-OLA was then functionalized with ascorbic acid (NP-ACP-OLA-AA). NP-ACP-OLA (1 g) was dispersed in 20.8 mL of ascorbic acid (0.1 M, pH = 7 adjusted with NaOH). After 5 minutes of stirring at room temperature, NP-ACP-OLA-AA were collected by centrifugation (12,500 rpm, 2 minutes, 10°C). NP-AA were prepared as control for biological assays through the functionalization of naked NPs with ascorbic acid (NP-AA), following the procedure previously described. The samples containing AA were frozen at −80°C to avoid its degradation.[20] Small quantities of

each sample were freeze-dried (Telstar Cryodos freeze-drier) for further characterization, and the rest of the sample was used for biological assays.

Characterization Techniques and Compositional Analysis of Doped ACP Nanoparticles

Fourier transform infrared (FTIR) spectra of powdered samples were recorded on a Tensor 27 (Bruker, Karlsruhe, Germany) spectrometer. Each sample (2mg) was mixed with 200 mg of anhydrous potassium bromide (KBr), set into a 12 mm diameter disc and pressed at 5 tons by a hydraulic press (Specac). Three discs were performed for each sample, and KBr disc was the blank reference. All the infrared spectra were recorded from 400 cm^{-1} to 4000 cm^{-1} at a resolution of 4 cm^{-1}. The nitrogen content of NP-ACP-OLA and ACP-OLA-AA NPs was measured by elemental analysis to quantify the amount of adsorbed OLA as well as the adsorption efficiency. This measurement was carried out with a Thermo Scientific Flash 2000 organic elemental analyser equipped with a microbalance (XP6, Mettler Toledo) from Centre for Scientific Instrumentation of the University of Granada (CIC-UGR). The amount of adsorbed ascorbic acid of NP-ACP-AA and NP-ACP-OLA-AA was quantified by UV–Vis spectroscopy at $\lambda = 265$ nm (Section S1 and Figure S1 of the Supplementary Material).

X-Ray powder diffractograms (XRPD) were recorded on a Bruker AXS D8 Advance diffractometer using Cu Kα radiation ($\lambda = 1.5418$ Å), from 8° to 60° (2θ) with a scan rate of 0.5 s step,$^{-1}$ step size of 0.02° with an HV generator set at 40 kV and 40 mA. Transmission electron microscopy (TEM) images, selected area electron diffraction (SAED), high-angle annular dark field-scanning transmission electron microscopy (HAADF-STEM) images, and energy-dispersive X-ray spectroscopy (EDS) elemental maps were acquired with STEM FEI TALOS F200X microscope equipped with a 4 Super-X SDDs (Thermo Fisher Scientific Waltham, MA, USA) from CIC-UGR. ACP-OLA-AA NPs were ultrasonically dispersed in ultrapure water, and then, some drops of the slurry were deposited on 200 mesh copper grids covered with thin amorphous carbon films. NP chemical composition (Ca, P, and K) was evaluated by ICP-OES (Inductively coupled plasma optical emission spectroscopy, Optima 8300, PerkinElmer, CIC-UGR). 10 mg of the powdered samples were dissolved in 1.5 mL of ultrapure nitric acid and then, the mix was made up to 50 mL with ultrapure water. Each sample was measured in triplicates at the emission wavelength for the quantification of each element, Ca (317.93 nm) and P (213.62 nm). The surface charge of the NPs (zeta potential, ζ, mV) was measured in Litesizer 500 (Anton Paar, Austria) through electrophoretic mobility and using disposable folded capillary cells.

Drugs Release Kinetic in PBS Media

The release kinetic of OLA and ascorbic acid from NP-ACP-OLA-AA was monitored by UV–Vis spectroscopy (Cary 100 Agilent Technologies, Santa Clara, CA, USA). Briefly, 0.9 mg of NPs were weighed in a quartz cuvette and then, 3 mL of PBS solution (pH=7.4) were added carefully to the cuvette. The absorbance curve from 200 nm to 400 nm was measured in continuous mode every half hour until reaching the plateau. The amount of released OLA and ascorbic acid was determined at wavelengths of 311 nm and 265 nm, respectively (Section S2 of the Supplementary Material).

The dissolution kinetic of free OLA was also evaluated by UV–Vis spectroscopy. For this purpose, 3 mL of OLA solution (100 ppm) in PBS were deposited in a quartz cuvette and the absorbance at 265 nm was measured in continuous until reach the plateau. The degradation rate of ascorbic acid (10.5 ppm) solution in PBS was also monitored at 311 nm. All measurements were performed in triplicates.

Cell Culture

MIA PaCa-2 and PANC1 human pancreatic ductal adenocarcinoma cell lines were purchased from the Center of Scientific Instrumentation (CIC-Granada University), and the murine pancreatic cancer cell line Panc02 was kindly provided by Dr. Lars Ivo Partecke, University of Greifswald, Germany. All the cell lines were grown in Dulbecco´s modified Eagle´s medium (DMEM) (Sigma-Aldrich, San Luis, EEUU) supplemented with 10% foetal bovine serum (Thermo Fisher, Waltham, Massachusetts, EEUU) and 1% penicillin–streptomycin (Sigma-Aldrich). Cells were maintained in monolayer culture in a 37 °C and 5% CO_2 atmosphere and passaged using 0.25% trypsin and 0.02% EDTA.

Cell Viability Assays

Cells were seeded at densities of 8×10^3 cells/well in PANC-1 and 2.5×10^3 cells/well in Panc02 and MIA PaCa-2 in 48 well plates (Thermo Fisher), incubated overnight, and exposed to DMSO (OLA solvent) (Thermo Fisher), OLA (different concentration ranges according to the cell line used), NPs with and without OLA, and ascorbic acid (Sigma-Aldrich) for 72h. Subsequently, the cells were fixed using 10% trichloroacetic acid for 20 minutes and washed thrice with distilled water. Later, the cells were stained using Sulforhodamine B (SRB, Sigma-Aldrich) for 20 minutes, being washed using three 1% acetic acid washes. Subsequently, the SRB dye was solubilized using Trizma® reagent (Sigma-Aldrich). Finally, the optical density (OD) of the dye was measured with a Titertek Multiskan colorimeter (Flow, Irvine, CA, USA) at 492 nm. The percentages of proliferation (Pf%) was calculated as: Pf% = (sample OD/negative control OD) × 100. To calculate IC_{50} values, nonlinear regression with viability curve fitting was performed using Prism 9.3. To calculate the synergistic index of the combination of AA and OLA, Compusyn 1.0 software was used.

In vitro Alizarin Red Staining

The NP-ACP-AA stock NPs were incubated for 1 minute with 2% alizarin red stain (prepared at pH 4.2, Sigma-Aldrich). Subsequently, two washes were performed with PBS centrifuging at 15,000 rpm.

For the observation of NPs cell internalization, 1.5×10^4 PANC-1 cells were seeded in 96-well plates and incubated overnight. The next day, the cells were treated with 100 mM NP-ACP-AA for 24 hours. The next day, the cells were washed twice with PBS and subsequently fixed using 95% methanol for 10 minutes at 4°C. Subsequently, the cells were stained using 2% alizarin red for 25 minutes in the dark. Finally, they were washed three times with water and visualized under DM IL LED microscope (Leica, Wetzlar, Germany).

Cell Migration Assay

PANC-1 cell line was seeded in 12-well plate (Thermo Fisher) and grown to 95–100% confluency in DMEM (Sigma-Aldrich) supplemented medium. Then, a vertical gap was manually performed using a pipette tip.[21] The following day, dead cells were removed using phosphate-buffered saline (PBS) and culture medium was substituted for DMEM without FBS to prevent cell proliferation. Then, an IC_{25} of OLA concentration (free and OLA-NPs) was added to the wells, and the cells were incubated for 72 h in which the migratory process was monitored using a DM-IL LED microscope (Leica). The percentage of migration was calculated by measuring the area free of tumor cells at different times using ImageJ software with the Chemotaxis and Migration Tool plugin (NIH, Maryland, USA).

DNA Fragmentation Assay (TUNEL)

TUNEL assay (Roche, Basel, Switzerland) was carried out on PANC-1 cells and sections of PANC-1 tumors from mice. Cells were seeded (1×10^5) in Culture Slides Chambers (Franklin Lakes, New Jersey, EEUU), incubated overnight, and treated with DMSO, NP-ACP-AA, OLA, and NP-ACP-OLA-AA at 100 μM doses (24 h). Cells treated with DMSO, and NP-ACP-AA were used as control. Then, cells were fixed in paraformaldehyde (4%) at RT for 1 h and washed with PBS. Tissue sections were deparaffinized with xylol and ethanol mixtures of decreasing concentrations (100, 95, 70%) and rehydrated. Subsequently, both cells and tissues were permeabilized with Triton X100 (0.1%) and sodium citrate solution diluted in PBS (0.1%) for 2 and 8 min, respectively. After washing the samples with PBS, an experimental positive control was generated using 10 U/mL DNase I (Sigma-Aldrich) for 10 min at RT. Finally, TUNEL test was carried out following the manufacturer's instructions.

Immunofluorescence Assays

For in vitro assays, 1.5×10^4 cells/well of the PANC-1 line were seeded in 96-well plates (Thermo Fisher) and incubated overnight. Subsequently, cells were treated with DMSO, NP-ACP-AA, OLA and NP-ACP-OLA-AA at a concentration of 100 mM for 24 hours. The next day, the cells were washed twice with PBS and fixed using 95% methanol for 5 minutes at −20°C. Subsequently, two washes were performed with PBS, and the cells were permeabilized for 10 minutes with 0.3% Triton X100 (Sigma-Aldrich) diluted in 0.1% PBS-tween. Later, the cells were blocked using 5% goat serum

diluted in PBS-tween for 30 minutes. After this step, the cells were incubated with the primary Murine anti-Ki67 antibody at a 1:50 dilution (BD 550609, New Jersey, EEUU) for 1 hour at room temperature. After three washes using PBS-Tween, the cells were incubated with a goat anti-mouse IgG-FITC secondary antibody at a 1:100 dilution (Santa Cruz Biotechnology, Dallas, Texas, EEUU) for 1 hour. Finally, three washes were performed using PBS-Tween and staining of cell nuclei was performed using Hoechst at a 1:1000 dilution. To analyze Ki67 labelling in mouse-derived tumor samples, the samples were fixed in formaldehyde and embedded in paraffin. Subsequently, they were deparaffinized and rehydrated (protocols explained later). After this, antigenic recovery of the samples was performed by incubating them in 10% citrate buffer for 20 minutes in a heat vaporizer. After cooling the samples for 10 minutes, the Ki67 labelling protocol was performed as explained above. Finally, the samples were mounted using ProLong Gold Antifade Mountant (Thermo Fisher). Fluorescence was visualized on a DM-IL LED microscope (Leica), and quantification of the Ki67 labelling foci was performed using ImageJ software (NIH).

Western Blot Assays

PANC-1 cells were washed twice with PBS and lysed with RIPA lysis buffer (Sigma-Aldrich). Protein concentration was determined using Bradford Reagent (Bio-Rad, Hercules, California, EEUU). For electrophoresis, 40 µg of proteins from each sample were heated at 95 °C for 5 min and separated in 12.5% SDS-PAGE gel. Fractions were transferred to nitrocellulose membranes, blocked for 1 hour at room temperature in 5% (w/v) BSA in TBS containing 0.1% Tween 20 (TBS-T) and co-incubated overnight at 4°C with the primary antibodies: γ-H2AX 1:1000 (Thermo Fisher) and β-actin-HRP 1:50,000 (Santa Cruz Biotechnology). Then, membranes were washed three times with TBS-T and incubated (1 h) with the horseradish peroxidase conjugated (HRP) anti-mouse secondary antibody 1:5000 (Santa Cruz Biotechnology). Proteins were visualized using the ECL system (Little Chalfont, United Kingdom) in the LAS-4000 mini equipment (GE Healthcare, Chicago, Illinois, EEUU). Further analysis, as well as image processing and quantification of the bands, was performed using the program Quantity One analytical software (Bio-Rad, Hercules, CA). γ-H2AX expression was normalized relative to the β-actin level of the cell lines.

In vivo Tumor Growth Assay

Male and female NOD SCID gamma (NSG) mice were generated by Scientific Instrumentation Center, University of Granada, and were used in the in vivo study. All mice (body weight: 20–25 g) were housed in cages with free access to water and food prior to the experiments and were maintained in controlled temperature, light, and humidity (22.0 ± 2°C, 12h light–dark cycle, and 40–70% relative humidity), under specific pathogen-free conditions with a sterile atmosphere controlled by HEPA filters. The study was approved by the Ethics Committee on Animal Experimentation of the University of Granada (Reference code: 16/01/2020/005) and performed according to its guidelines. Tumors were induced by subcutaneous injection of 9×10^5 cells derived from PANC1 cell line into the right flanks of NSG mice. When the tumor was palpable, animals were randomly divided into four groups (n = 8–10 mice per group, selecting the mice that induced the tumor): PANC1 mice were treated with free OLA (group II) and OLA solvent as control (group I); and with NP-ACP-OLA-AA (group IV), using NP-ACP-AA as control (group III). OLA solvent was 5% DMSO, 40% PEG300, 5% Tween-80 and 50% saline, while nanoparticles were suspended in the saline serum. All the treatments were administered intraperitoneally. OLA was administered both free and adsorbed into NPs at a concentration of 25 mg/kg every 3 days up to a total of 10 cycles of treatment and the same volume of OLA solvent and free-cargo NPs concentration was used in control and NP-ACP-AA control groups. Weights and deaths were carefully recorded throughout the period, and the tumor volume was measured using a digital caliper. The tumor volume (mm^3) was calculated as follows: $V\ (mm^3) = (a \times b^2 \times \pi)/6$.

Histological Assays

Tumors were extracted from the mice, fixed in formaldehyde, and embedded in paraffin and cut with a rotation microtome (Leica).

For haematoxylin-eosin staining, the sections were stained with haematoxylin–eosin (Merck, Darmstadt, Germany). For the detection of NPs in the samples, after rehydration the tissues were stained for 2 minutes with 2% alizarin red (Sigma-Aldrich). Subsequently, the staining was dried, and 20 washes were performed using 100% acetone.

Table 1 Human Primers Used for Amplification of the Genes Analyzed

Gene		Primer	Tm°
STAT3	Forward	GGTACATCATGGGCTTTATC	58.3
	Reverse	TTTGCTGCTTTCACTGAATC	60.6
TFG-β1	Forward	CCCACAACGAAATCTATGAC	59.4
	Reverse	TGTATTTCTGGTACAGCTCC	56.8
MMP-9	Forward	CTTAGATCATTCCTCAGTGC	56.4
	Reverse	CGAGGACCATAGAGGTG	56.4
EGFR	Forward	TCTTAAAGACCATCCAGGAG	58.3
	Reverse	ATCTGCAGGTTTTCCAAAG	59.3
PARP1	Forward	AAAAGGAGGTGGAAAAGATG	59.6
	Reverse	GCTAAGAACAACTCCTGAAG	55.7
GAPDH	Forward	TCGGAGTCAACGGATTTG	62.4
	Reverse	CAACAATATCCACTTTACCAGAG	59.1

Subsequently, the samples are washed 20 times in a 50% xylene-acetone solution and were finally rinsed in xylene. Finally, the samples were mounted in Organo/limonene Mount (Sigma-Aldrich).

RT-qPCR Assays

Murine tissues were preserved in RNAlater (Thermo Fisher) at −80°C. Once stabilized, 20 mg of each tumor was homogenized using a T10 basic ULTRA-TURRAX blender (IKA, Staufen, Germany). RNA extraction was performed using the RNeasy Mini Kit (Qiagen, Hilden, Germany), performing RNA purification using RNase-Free DNase Set (Qiagen) following the manufacturer's instructions. The RNA concentration of each sample was quantified using Nanodrop 2000 (Thermo Fisher). The reverse transcription was performed using the Reverse Transcription System kit (Promega, Madison, Wisconsin, EEUU) following the manufacturer's instructions. Finally, quantitative RT-PCR was performed using TB Green® Premix Ex Taq™ II (Takara Bio, Kusatsu, Japan). The primers used are listed in Table 1. Gene expression between samples was normalized using the GAPDH gene. All quantitative qPCR assays were performed in an ABI 7900 system (SeqGen, Torrance, CA, EEUU), and the $2^{-\Delta\Delta Ct}$ method was applied to calculate relative expression levels.

Statistical Analysis

The statistical tests used were performed using SPSS v.28.0 software (SPSS, Chicago, IL, USA). Thus, for the general comparison between the two samples, Student's *t*-tests were used. For the comparison between several samples, one-way (for univariate comparisons) and two-way ANOVA (for comparisons of two variables) with Tukey's post-hoc test was performed, considering data with $p < 0.05$ significative. A Kaplan–Meier method was used to determine the probability of mice survival, and the Log rank test was used to compare the fraction of surviving mice between groups.

Results

Synthesis and Characterization of Nanoparticles

The dual functionalization of the NPs was carried out according to the steps illustrated in Figure 1. First, calcium phosphate NPs were functionalized with OLA (NP-ACP-OLA), a hydrophobic molecule with poor water solubility.[22] The adsorption of OLA was carried out for 24 hours to ensure the maximum loading capacity, according to our previous studies aimed at the functionalization of calcium phosphate NPs with doxorubicin, a poor water-soluble chemotherapeutic agent.[23,24] Then, the resulting nanoassembly was functionalized with ascorbic acid by incubation for a short period of time (5 minutes) since AA possess high chemical instability to oxygen, temperature, humidity, and light.[20] The resulting dual nanoplatform was referred to as NP-ACP-OLA NPs (Figure 1).

The successful functionalization was evaluated by FTIR spectroscopy and ζ-potential measurements. FTIR spectra (Figure 2A) of naked NPs and functionalized (NP-ACP-OLA and NP-ACP-OLA-AA) show the typical poorly defined

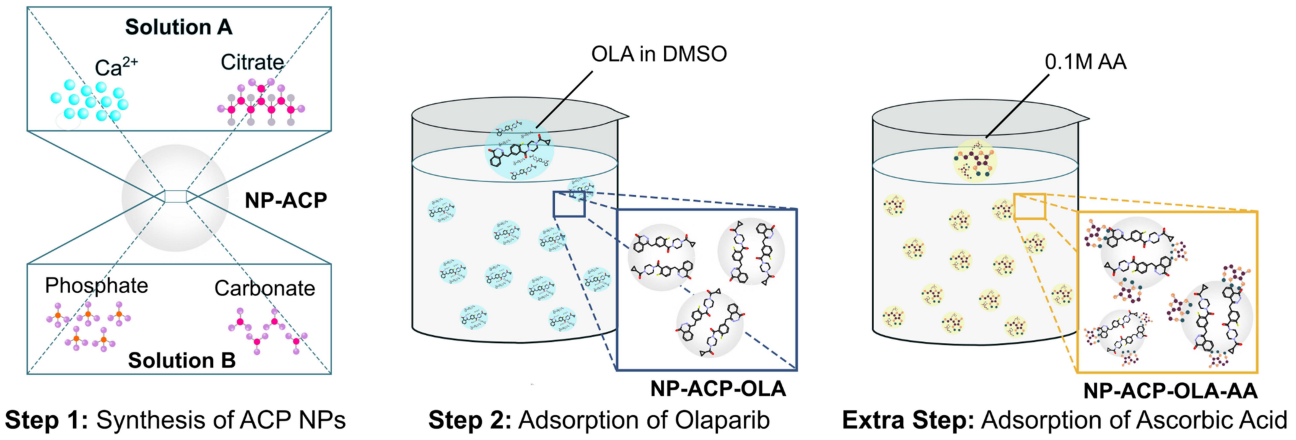

Figure 1 Graphical sketch of the NP functionalization to obtain the dual nanosystem. It consists of two steps: (i) OLA adsorption (NP-ACP-OLA) and ii) the subsequent ascorbic acid adsorption (NP-ACP-OLA-AA).

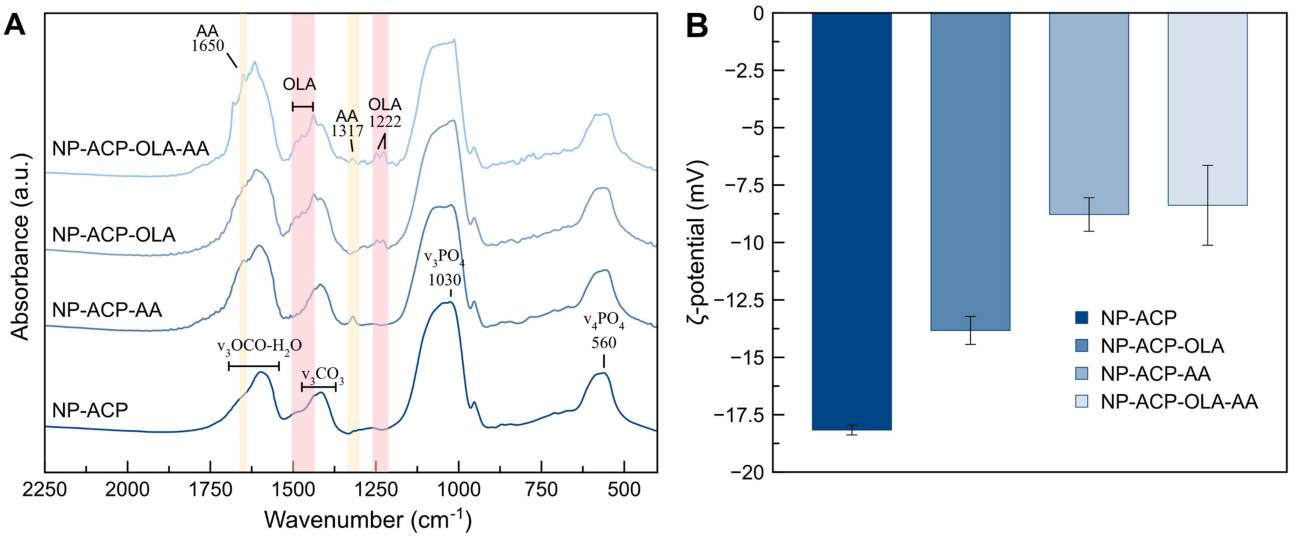

Figure 2 Characterization of the nanosystems: (**A**) FTIR spectra of naked ACP NPs and functionalized with ascorbic acid (NP-ACP-AA), OLA (NP-ACP-OLA) and both molecules (NP-ACP-OLA-AA). The FTIR spectra were normalized by the maximum intensity (at ca. 1030 cm^{-1}) and vertically offset for the sake of clarity. The bands ascribed to OLA and ascorbic acid are highlighted in pink and yellow, respectively. (**B**) ζ -potentials of the functionalized (NP-AA, NP-ACP-OLA and NP-ACP-OLA-AA) and non-functionalized NPs for comparison. The graph displays the mean average and their standard deviation.

phosphate absorption bands characteristics of amorphous calcium phosphate with additional peaks corresponding to citrate, carbonate, and water.[19] The FTIR spectra of NP-ACP-AA and NP-ACP-OLA-AA (Figure 2A) also display two peaks at ~1317 cm^{-1} (C-H wagging) and 1650 cm^{-1} (C=C ring stretching) attributed to ascorbic acid,[25] confirming the successful adsorption of this molecule on NP surface. OLA signals (ie, 1222 and 1438 cm^{-1})[26] are distinguished in the FTIR spectra of NP-ACP-OLA and NP-ACP-OLA-AA, indicating that OLA adsorption was also effective. The ζ-potential measurements were carried out to investigate the surface charge modification associated with NP functionalization (Figure 2B). The mean ζ-potential of the non-functionalized ACP NPs was negative (−18 mV) due to citrate, which remains on the surface of the NPs.[27] ζ-potential increased to −14 mV after the coupling with OLA. The increase in ζ-potential was more pronounced for AA adsorption (NP-ACP-AA, Figure 2B), being the reduction on surface charge similar to that observed after the dual functionalization (NP-ACP-OLA-AA). These findings confirmed the effective binding of AA and OLA on the surface. In fact, the elemental analysis revealed the presence of a 13.2 ± 0.9 wt.% of OLA in NP-ACP-OLA-AA, achieving an adsorption efficiency of 75.4 ± 10.5%. On the other hand, ascorbic acid quantification by UV-spectroscopy indicated a very low load (1.2 ± 0.7 wt.%), most probably due to the few remaining active sites on the ACP NPs surface after OLA adsorption.

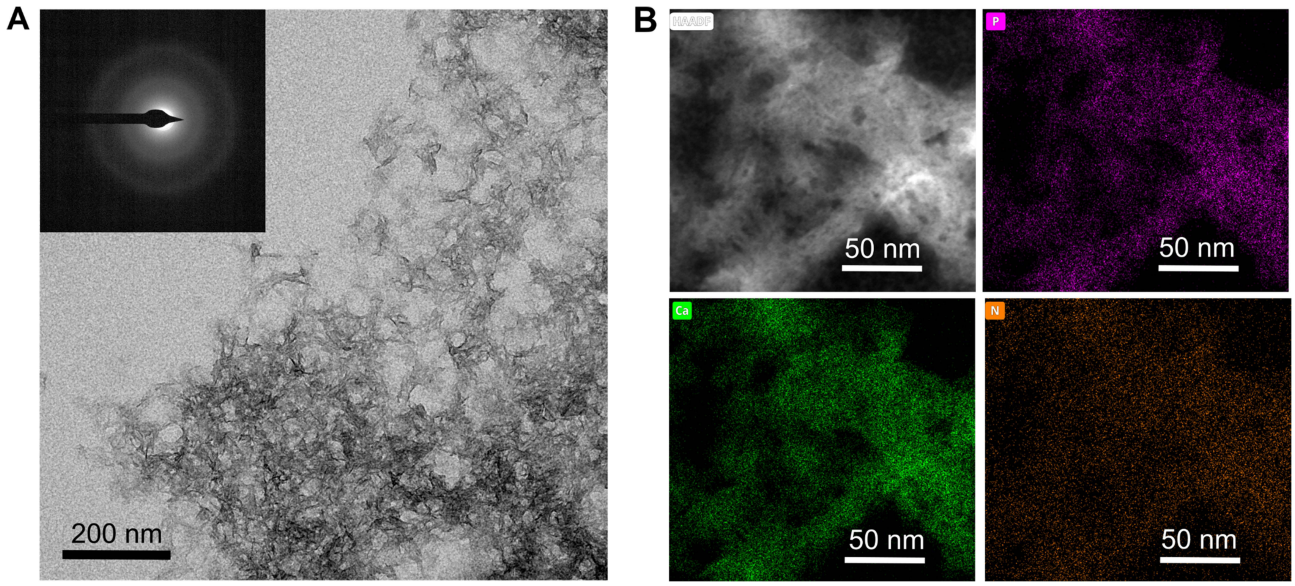

Figure 3 Electron Microscopy analysis of the NPs: (**A**) TEM micrograph of NP-ACP-OLA-AA. Inset displays the SAED pattern of the NPs. Scale bar=200nm. (**B**) HAADF-STEM image and EDS maps of NP-ACP-OLA-AA showing the calcium (green), phosphorus (pink) and nitrogen (Orange) distribution along the NPs. Scale bar = 50 nm.

The morphology of NP-ACP-OLA-AA was also evaluated by TEM (Figure 3). NP-ACP-OLA-AA exhibited needle-like morphology with a length below 20 nm. The poorly defined morphology is due to the transition from amorphous precursor to poor crystalline apatite during the functionalization process.[24] In fact, SAED pattern (inset Figure 3A) shows diffuse rings confirming the amorphous or low crystallinity degree of NP-ACP-OLA-AA.[19] The individual chemical maps (Figure 3B) obtained by EDS demonstrated that nitrogen (orange) of OLA molecules is homogenously distributed within the NPs, along with calcium (green) and phosphorus (purple).

Release Drug Kinetics of the Active Molecules

The delivery of OLA and ascorbic acid from NP-ACP-OLA-AA in PBS medium was monitored by UV–Vis spectroscopy (Figure 4). This technique allowed the simultaneous quantification of the two molecules by monitoring the absorbance at 311 nm (OLA) and 265 nm (AA) (Fig. S2). The experimental cumulative release of OLA was fitted to a semi-empirical Power law's model, ($y(t)=a\cdot t^{b}$, $b\leq 1$), where "a" parameter is related to the release velocity and "b" define the drug release mechanism.[28] OLA desorption from the NPs had a slower release profile than free OLA dissolution (Figure S3).

The behavior of AA is completely different. The concentration of AA in solution decreases with the time (Figure 4). The degradation of AA followed an exponential decay according to the equation $y(t)=e^{-t/\tau}$, where τ corresponds to half lifetime of the molecule. Interestingly, the half lifetime of AA released from NP-ACP-OLA-AA (τ=15.261 h) is nine times higher than half lifetime of free AA in dissolution (τ=2.678 h) (Figure S3). In fact, free AA was degraded in 12 h, while AA released from NP-ACP-OLA-AA remained for up to 60 h. This confirmed the protective effects of calcium phosphate NPs that ensure AA availability for almost the entire time of in vitro cell experiments (72 hours).

Cytotoxic Effect of Olaparib Decorated Nanoparticles in Pancreatic Cancer Cell Lines

Panc02, PANC-1, and MIA PaCa-2 cell lines were treated with NP-ACP-OLA and NP-ACP-OLA-AA to determine their cytotoxic effect (Figure 5A–C). NP-ACP-OLA induced important cytotoxic effects in the three cell lines tested (Figures 5A–C). Interestingly, NP-ACP-OLA-AA enhanced the effect of OLA drug by decreasing IC_{50} by 51, 56, and 28% in Panc02, PANC-1, and MIA PaCa-2 lines, respectively (Figure 5C). The toxicity of NP-ACP and NP-ACP-AA was also tested in all the cell lines as controls, resulting in some inhibition of proliferation in Panc02 cell lines (ca. 15% of viability reduction). The toxicity of the respective controls (DMSO for free drug, NP-ACP for NP-ACP-OLA and NP-ACP-OLA-AA for NP-ACP-OLA-AA) was

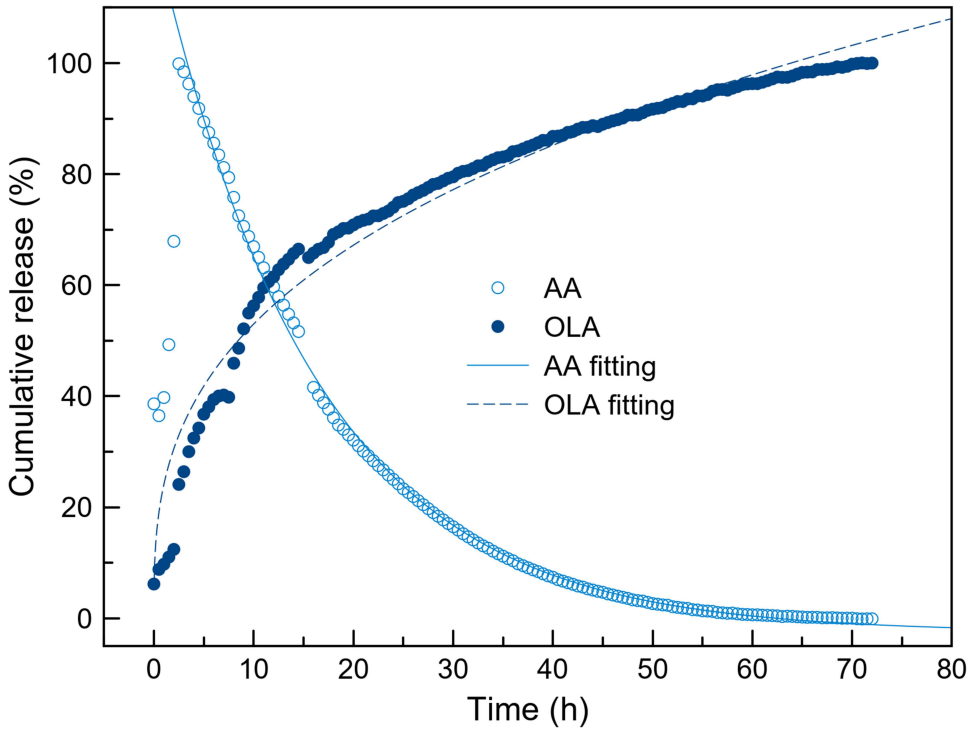

Figure 4 Release kinetics of OLA and AA from the NPs. Cumulative release (%) of OLA (solid symbols) and AA (empty symbols) from NP-ACP-OLA-AA in PBS media. AA is degraded in solution once detached from the surface of the NPs. Dashed line represents the theoretical curves estimated according to Power law's approximation ($y(t) = a\ t^b$), where the amount of drug in time ($y(t)$) depends on the effective diffusion constant a, time (t) and the drug release mechanism. Solid line represents the theoretical curves estimated according to an exponential decay of the drug: $y(t)=\exp(-t/\tau)$, τ corresponds to half lifetime of the drug.

subtracted to estimate the normalized IC_{50} values (NV, Figure 5C) to understand the real effect of the treatment. As a result, NP-ACP-OLA (22.58 and 24.84 µM) was found to be less effective than the free drug (11.15 and 15.45 µM) against Panc02 and MIA PaCa-2 cell lines, respectively. The cytotoxic effect exerted by NP-ACP-OLA-AA in MIA PaCa-2 cells (15.62 µM) was similar to that obtained for the free drug (15.45 µM). By contrast, NP-ACP-OLA-AA induced a significantly higher cytotoxic effect than the free drug in Panc02 and PANC-1 cell lines, being the later the most resistant cell line against OLA (IC_{50} was 7.5 and 8.5 times greater than in MIA PaCa-2 and Panc02, respectively) (Figure 5C).

The cells after the treatments were also analyzed by optical microscopy (Figure 5D and E). After 72 hours of treatments, OLA and NP-ACP-OLA-AA produced a widening of the cells, appearing clear symptoms of cell membrane damage (marked with yellow arrows in Figure 5D. NPs used as control (NP-ACP-AA) were stained with alizarin-red, which is a dye commonly used to stain calcium salts, with the aim of identifying the internalization and further accumulation of NPs inside the cells (Figure 5E). Aggregates of red-stained NPs were found in the cell cytoplasm, confirming that the NPs were able to penetrate the cells (Figure 5E). Based on these interesting in vitro results, the most effective dual nanoplatform (NP-ACP-OLA-AA) and the most sensitive cell line (PANC-1) were selected to perform further in vitro and in vivo experiments. The NP-ACP-AA system, which contained one of the chemo-agents but exhibiting null cytotoxic effect against PANC-1 cells (Figure 5A) was used as control.

The Combination of AA and OLA Exerts Synergistic Cytotoxic Effect in vitro

The PANC-1 cell line was exposed to AA (75 and 100 µg/mL), OLA (15 µM), and their combination (AA-OLA) to determine the existence of a synergistic effect. As shown in Figure 6A, AA did not induce toxicity at these concentrations. Subsequently, PANC-1 cells were treated with a combination of both (AA-OLA) showing a greater cytotoxic effect (real inhibition) than the relative inhibition of their combination (theoretical inhibition) (Figure 6B). This effect was corroborated by the synergistic index (CI) which indicated that the combination of 75 µg/mL of AA and 15 µM OLA exerted synergy in vitro (CI = 0.327) (Figure 6B).

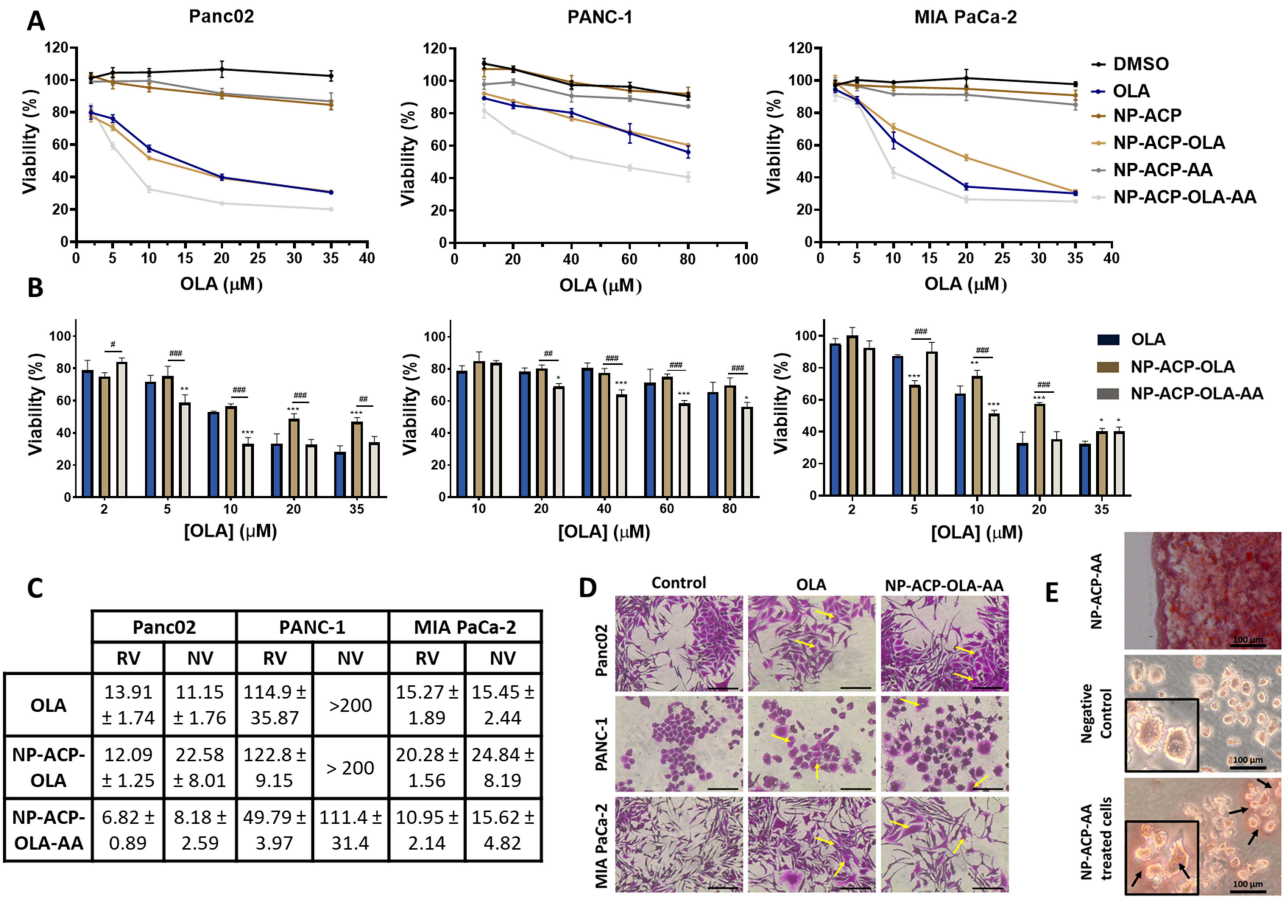

	Panc02		PANC-1		MIA PaCa-2	
	RV	NV	RV	NV	RV	NV
OLA	13.91 ± 1.74	11.15 ± 1.76	114.9 ± 35.87	>200	15.27 ± 1.89	15.45 ± 2.44
NP-ACP-OLA	12.09 ± 1.25	22.58 ± 8.01	122.8 ± 9.15	> 200	20.28 ± 1.56	24.84 ± 8.19
NP-ACP-OLA-AA	6.82 ± 0.89	8.18 ± 2.59	49.79 ± 3.97	111.4 ± 31.4	10.95 ± 2.14	15.62 ± 4.82

Figure 5 Cell cytotoxicity of free and adsorbed OLA in different pancreatic adenocarcinoma cell lines. (**A**) Cell lines of pancreatic adenocarcinoma (Panc02, PANC-1, and MIA PaCa-2) were exposed to increasing concentrations of OLA, free or adsorbed on NPs. Cell viability of the corresponding controls (DMSO, NP-ACP and NP-ACP-AA) is also shown. (**B**) Graphical representation of the normalized proliferation values in cell lines treated with free OLA, NP-ACP-OLA and NP-ACP-OLA-AA after subtracting the effect of their controls: DMSO, NP-ACP and NP-ACP-AA, respectively. Data are represented as the mean ± SD (n=3). *p ≤ 0.05, **p ≤ 0.01, ***p ≤ 0.001; #Were used to indicate the significant differences in cell viability between NP-ACP-OLA and NP-ACP-OLA-AA groups. #p ≤ 0.05, ##p ≤ 0.01, ####p ≤ 0.001. (**C**) IC_{50} values (in μM) obtained in the cell lines after being treated with OLA, NP-ACP-OLA, and NP-ACP-OLA-AA. The real value (RV) and the normalized value (NV) represents, respectively, the IC_{50} without or with subtraction of the control toxicities. (**D**) Optical micrographs of cells treated with OLA or NP-ACP-OLA-AA, showing cell enlargement compared to the control. Scale bar = 100 nm. (**E**) Optical micrograph of a drop containing red-stained nanoparticles (NP-ACP-AA) and micrographs of PANC-1 cells without treatment or treated with NP-ACP-AA for 24 hours and then stained with alizarin red. Scale bar = 100 nm. Pictures were collected with a 20X objective.

Dual Nanoparticles Inhibited Cancer Cell Migration and Ki67 Expression

To compare the effect of free OLA and NP-ACP-OLA-AA on PANC-1 cell migration, a phenomenon related to PARP1 inhibition, we exposed these cells to both treatments for 72 h. As shown in Figure 6C, NP-ACP-OLA-AA significantly inhibited cell migration at 48 and 72 hours relative to untreated cells, while free OLA inhibited migration only at 72 hours, with no significant differences compared to the effect exerted with NPs. On the other hand, we checked by immunofluorescence the expression of Ki67 in PANC-1 cells after being treated with the free drug free or with the dual nanosystem. The results showed that both OLA and NP-ACP-OLA-AA (OLA concentration of 10 μM) significantly reduced Ki67 expression compared to control cells ($p < 0.01$ and $p < 0.001$, respectively), without any significant differences between the two treatments (Figure 6D and E).

Apoptosis and Genotoxicity Induced by NP-ACP-OLA-AA Dual Nanoparticles

To determine the mechanism by which the NPs exerted their cytotoxic effect we carried out a TUNEL assay. As shown in Figure 6F, NP-ACP-OLA-AA induced a significantly greater proapoptotic effect in PANC-1 cells compared to free drug ($p < 0.001$). This effect was demonstrated by analyzing the percentage of positive nuclei for TUNEL, where NP-ACP-OLA-AA generated a greater induction of early apoptosis (86%) compared to the other conditions tested. As this apoptosis could be due to the generation of DNA damage, genotoxicity was analyzed quantifying the phosphorylated γ-

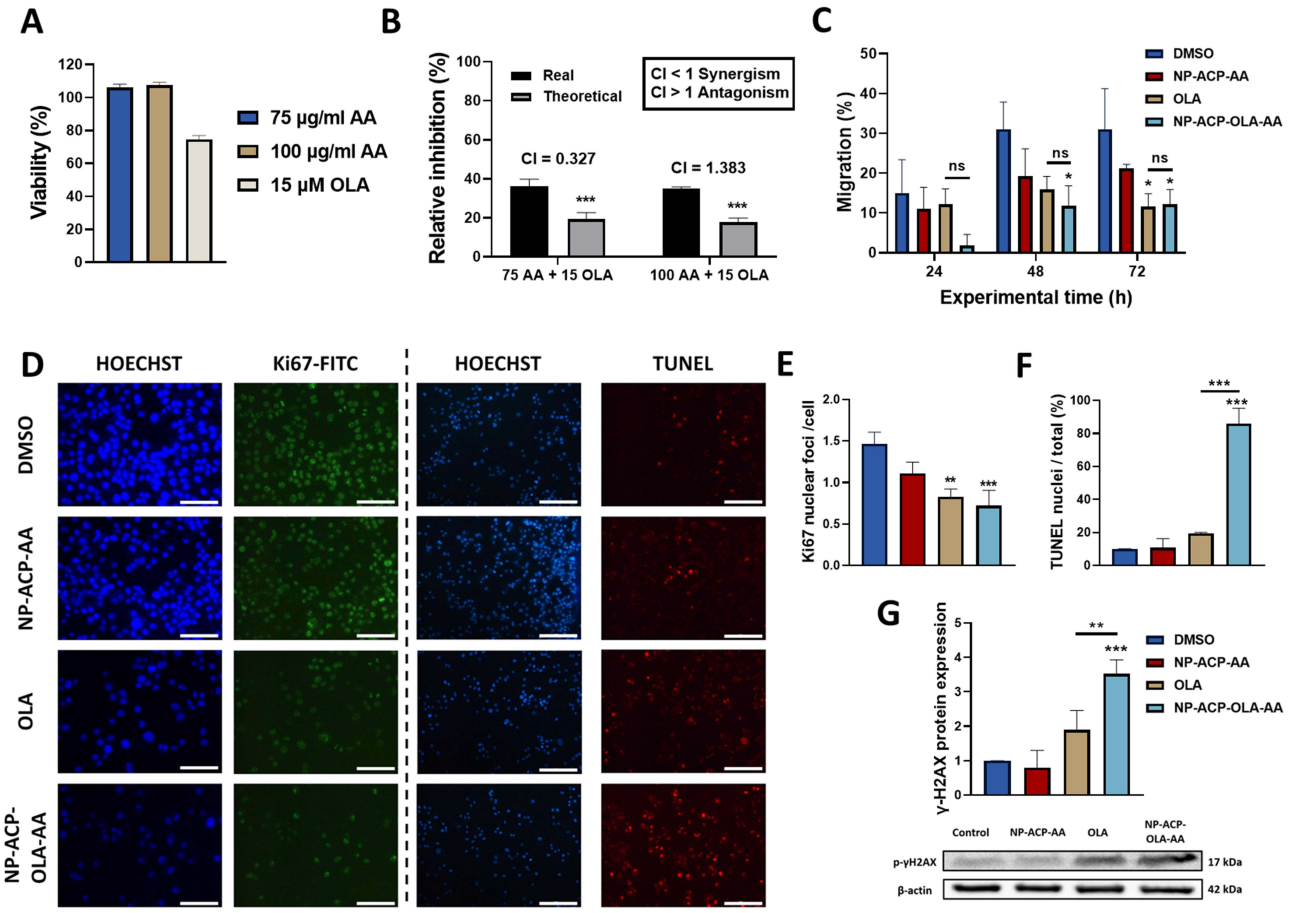

Figure 6 In vitro synergistic effect of OLA and AA and evaluation of the cytotoxic mechanisms. (**A**) Cytotoxic activity of ascorbic acid (75 and 100 µg/mL) and OLA (15 µM) against PANC-1 cell line after 72 hours of exposure. (**B**) Graphical representation of the real and theoretical inhibition (sum of both treatments separately) exerted by the combination of this AA and OLA doses in vitro and values of the combinatorial index (CI) obtained after combining both treatments in PANC-1 cell line. (**C**) Cell migration of PANC-1 treated with OLA, NP-ACP-OLA-AA, and their corresponding controls (DMSO and NP-ACP-AA) for 72 hours. (**D**) Representative immunofluorescence microscopy images of Ki67 protein expression and after performing a TUNEL assay treating PANC-1 cells with 100 µM of each treatment for 24 hours. Pictures were collected with a 10X objective. Scale bar = 200 nm. (**E**) Graphical representation of the Ki67 nuclear foci detected in each condition relative to the number of cells. (**F**) Graphical representation of the quantification of TUNEL-stained nuclei in comparison to the total nuclei. Nuclear staining was performed using Hoechst. Images were collected through a 10X objective. (**G**) Western blot analysis of phosphorylated γ-H2AX after 24-hour treatment of PANC-1 cells with OLA, NP-ACP-AA, and NP-ACP-OLA-AA NPs. All the data are presented as mean ± S.D (n=3). *p ≤ 0.05, **p ≤ 0.01 and ***p ≤ 0.001.
Abbreviation: ns, not significant.

H2AX expression using Western Blot. As shown in Figure 6G, NP-ACP-OLA-AA generated a significant increase (86%) in PANC-1 cells genotoxicity compared to free OLA after 72 hours of treatment ($p < 0.01$).

In vivo Tumor Growth Inhibition by Olaparib Decorated Nanoparticles

The effectivity of the dual nanosystem was also demonstrated in vivo in NSG mice with PANC-1 induced tumors. As shown in Figure 7A, control animals treated with the solvent (CTRL) and with OLA-free NPs (NP-ACP-AA) showed similar final tumor volumes with no significant differences between them. By contrast, OLA treatment produced a decrease of tumor volume (28.3%), which was statistically significant at the last treatment cycle. Interestingly, the dual nanosystem NP-ACP-OLA-AA induced the greatest decrease of tumor volume (59.1%), representing a significant decrease of tumor growth (30%) compared to free OLA. In addition, any differences in tumor growth were observed between the control groups in terms of survival (CTRL vs NP-ACP-AA). In contrast, the survival of mice treated with NP-ACP-OLA-AA was higher (78%) compared to control groups and free OLA treatment (50 and 44%, respectively) (Figure 7B). Histological analysis of the tissues obtained by haematoxylin-eosin showed that treatment with NP-ACP-OLA-AA produced large voids in the tumor sinus, losing its compact histology. On the other hand, staining of the tissues with alizarin red showed that NPs were accumulated in the tumor sinus (Figure 7C).

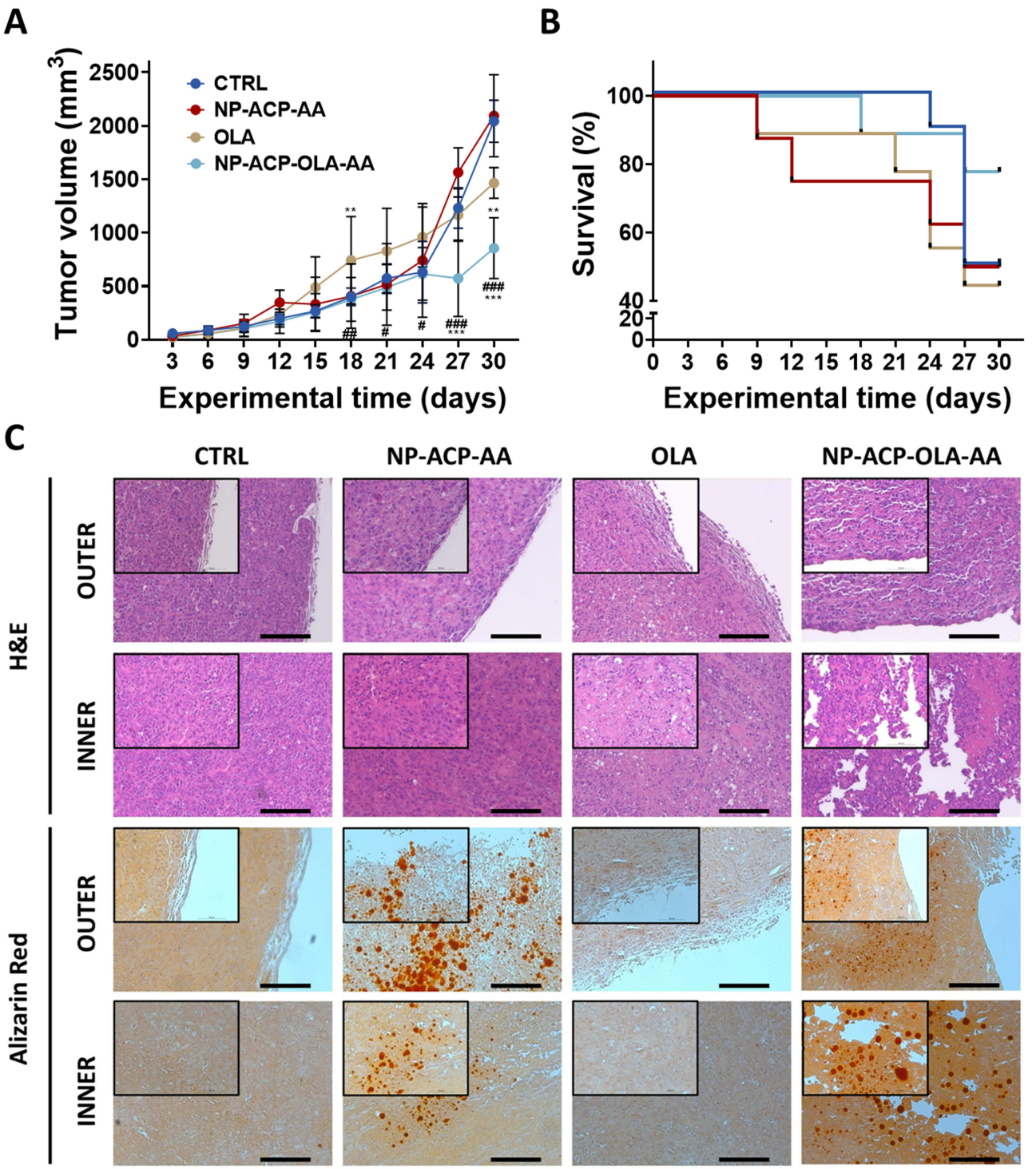

Figure 7 In vivo results in NSG mice with PANC-1 induced tumors. Tumor growth (**A**) and survival of mice (**B**) after CTRL, NP-ACP-AA, OLA, and NP-ACP-OLA-AA treatments. All the data are represented as mean ± S.D (n= 8–10). $^{**}p \leq 0.01$, $^{***}p \leq 0.001$ compared to the control group (CTRL); $^{\#}p \leq 0.05$, $^{\#\#}p \leq 0.01$, $^{\#\#\#}p \leq 0.001$ comparing the tumor growth of OLA and NP-ACP-OLA-AA groups. (**C**) Histological evaluation of the tumoral tissue using haematoxylin-eosin staining and the penetration of the NPs in the tumoral tissue using alizarin red staining. Scale bar = 500 nm.

Gene expression analysis of the extracted tumors showed that mice treated with NP-ACP-OLA-AA had lower STAT3, EGFR, and PARP1 gene expression compared to the control group, with significantly lower expression of the MMP-9 and EGFR genes compared to the group treated with free OLA (Figure 8A). Finally, the analysis of Ki67 expression in tumor tissues using immunofluorescence showed no significant differences in the number of Ki67-labeled

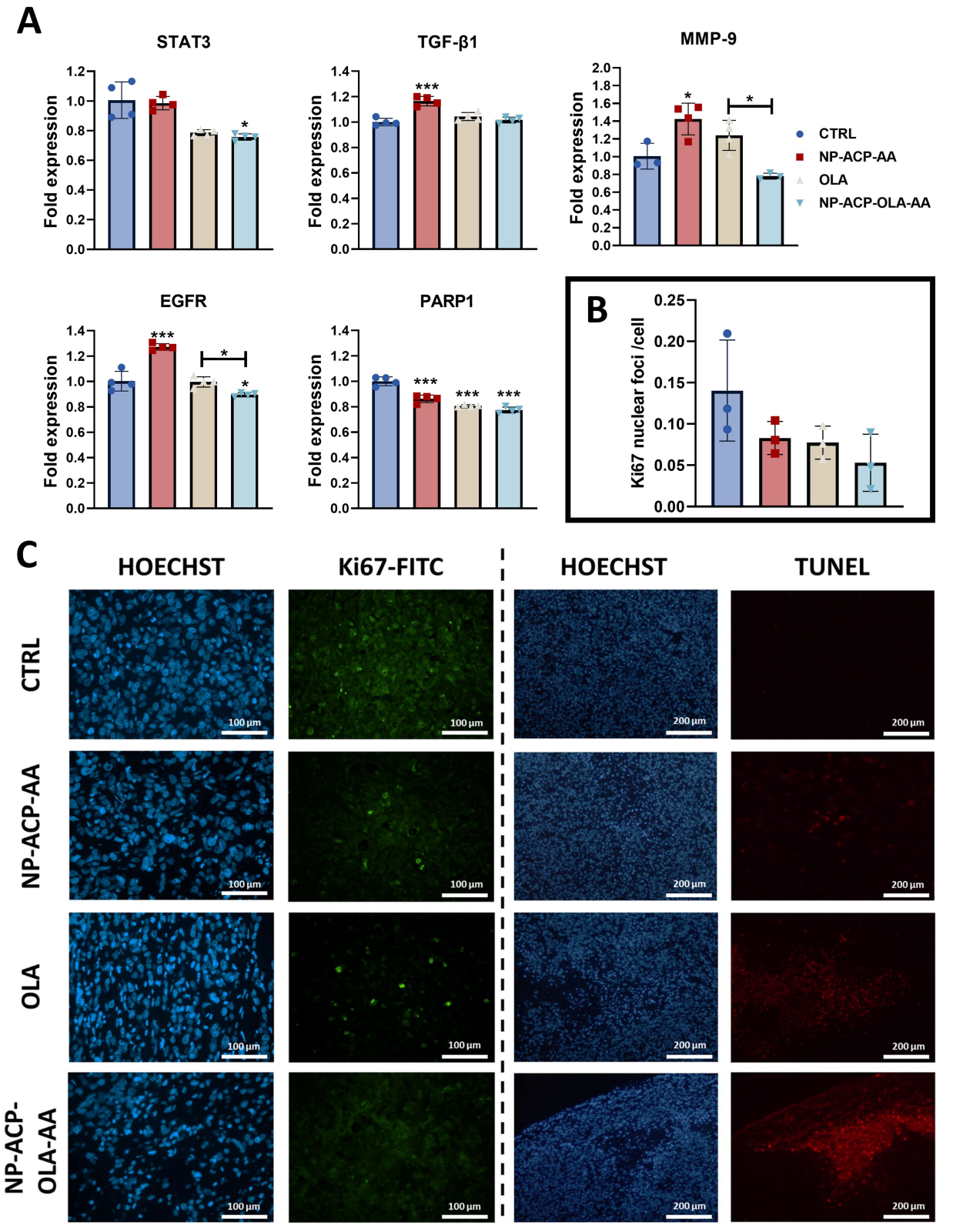

Figure 8 Histological and gene expression analysis of excised tumors. (**A**) Gene expression analysis of cellular malignancy marker genes carried out by RT-qPCR in tumors derived from the experimental groups tested. All the data are represented as mean ± S.D (n=3). *p ≤ 0.05, **p ≤ 0.01 and ***p ≤ 0.001 compared to the control. Significant differences between different groups have been pointed out. (**B**) Quantification of protein expression of the proliferation marker Ki67 in tumors excised from mice of the different experimental groups and (**C**) images obtained after performing the Ki67 immunofluorescence experiment (green fluorescence) and a TUNEL experiment (red) for the detection of apoptosis in situ. Sections were counterstained with Hoechst (blue). Images were collected at 10X magnification. The scale bar is indicated in the corresponding images.

nuclei in the experimental groups tested (Figure 8B and C). In addition, analysis of early apoptosis in histological sections indicated that NP-ACP-OLA-AA significantly increased the apoptotic potential of the drug (Figure 8C).

Discussion

Nanotechnology has emerged as a promising alternative in the treatment of some aggressive cancers with low survival rate, as pancreatic cancer. OLA-containing NPs have been assayed in breast,[11,29,30] small cell lung,[31] prostate,[32] and pancreatic cancer with BRCA2 mutation with different results depending on the type of tumor and the nanoformulation used. The co-administration of drugs is a promising strategy to develop more effective treatments.[8,10] In this work, calcium phosphate nanoparticles were efficiently functionalized with two chemo-agents, OLA and AA. NP-ACP-OLA-AA provides a slow and delay AA degradation, allowing the simultaneous release of both compounds up to 72 hours. This remarkable result assures the protection and presence of AA during almost all in vitro treatment and thereby, allows both drugs to act synergistically in a spatio-temporal synchronized manner. This interesting effect may explain the highest cytotoxicity effect of NP-ACP-OLA-AA in several pancreatic cancer cell lines compared to free OLA, NP-ACP-OLA and NP-ACP-AA. Despite of a low payload of AA (around 1%) on the surface, these nanosystems were generally more effective than the AA-free (OLA and NP-ACP-OLA), obtaining IC_{50} values that were 50, 56, and 28% lower in the Panc02, PANC-1, and MIA PaCa-2 lines compared to free OLA, respectively. These results are consistent with the previous obtained by Ma et al who showed that the co-administration of AA and OLA induced a "BRCAness" effect in ovarian cancer, reducing the expression of proteins involved in DNA damage repair by homologous recombination (RAD51, BRCA1, and BRCA2) and increasing the cytotoxic effect exerted by PARP inhibitors such as OLA.[33]

Nanoparticle internalization also explains the highest cytotoxicity of NP-ACP-OLA-AA in cancer cell lines. Previous works demonstrated that calcium phosphate nanoparticles are internalized via endocytosis.[34] Iafisco et al pointed out that Ap nanoparticles functionalized with doxorubicin were endocytosed and once inside the cell, DOXO was released from the NPs and translocated to the nucleus possibly through the formation of a DOXO–proteasome complex.[35] In our study, the internalized nanoparticles may release OLA and AA inside the cells triggering to cell death. The higher cytotoxicity of NP-ACP-OLA-AA respect to NP-ACP-AA or NP-ACP-OLA confirmed the synergistic effect of both compounds. This effect could be related to the AA oxidation that produces hydrogen peroxide which enters tumor cells through peroxyporins, causing oxidative stress and DNA damage. In addition, the PARP1 enzyme inhibition (involved in DNA repair) caused by PARPi (OLA) induced a synergistic effect.[36]

On the other hand, it has been shown that PARP1 inhibition can reduce cell migration capacity in hepatocellular, cervical, and pancreatic cancer cells.[37–39] This phenomenon has been widely related to tumor progression, invasiveness, and the generation of metastasis in PC.[40] Dual nanoparticles showed an inhibitory effect on cell migration like the free drug. In addition, NP-ACP-OLA-AA induced an increase in the apoptosis compared to free OLA (86.05 vs 19.84% of apoptotic induction). This cytotoxic effect of NPs resulted in a greater induction of genotoxicity (analyzed through the increased expression of p-γ-H2AX) in the PANC-1 cells, supporting previous studies where OLA-containing NPs potentiated genotoxicity induction by causing an increase in cell apoptosis compared to free drug.[41] Finally, our in vitro results showed that treatment with free or adsorbed OLA on the NPs (in combination with AA) produced a significant decrease of Ki67 expression. These increases may be attributed to the different kinetic profiles displayed by OLA when it is detached from nanoparticles, in comparison with free OLA solution. As depicted in Figure 4, the delivery of OLA from nanoparticles exhibited a slower release pattern than the free drug. This prolonged release of OLA ensures an extended cellular uptake over time, thereby guaranteeing enhanced effectiveness and efficiency of the treatment. In addition, these results are in agreement with those obtained by Nakamura et al who found that OLA-treated oral squamous cell carcinoma cells had lower gene expression of malignancy-related markers, including Ki67.[42]

These interesting in vitro results of NP-ACP-OLA-AA were confirmed in vivo. Previous studies demonstrated a strong in vivo tumor growth inhibitory effect using OLA-containing NP in breast and lung cancer.[11,43] Recently, some OLA nanoformulations with ferromagnetic properties have enhanced their efficiency by hyperthermia decreasing tumor growth (up to 80%) and increasing the time required (60%) to quadruple tumor size compared to free drug.[43,44] However, one concern of ferromagnetic materials is their biocompatibility. Hence, other stimuli-responsive nanoformulation based on biomaterials, such as our biomimetic calcium phosphate nanoparticles, has been proposed as a promising

strategy.[45] Hence, our results involving tumors induced from PANC-1 cells in NSG mice and treated with NP-ACP-OLA-AA showed a significant tumor volume reduction (up to 59%), while free OLA only achieved a 30% tumor volume reduction compared to control mice. Treatment with naked-NPs showed any significant differences compared to the control. Interestingly, treatment with NP-ACP-OLA-AA induced an increase in survival (28%) compared to all the other conditions tested. The effects exerted on the reduction of tumor volume were supported by the analysis of histological sections where a higher induction of apoptosis was observed in tumors treated with OLA-adsorbed NPs compared to free drug. Meanwhile, analysis by haematoxylin-eosin showed that OLA-loaded NPs generated a large tissue disruption, showing a large cytotoxic effect in the tumor sinus. Analysis of tumor tissues by alizarin red showed a large accumulation of calcium in tumor tissues of NPs-treated treated mice (NP-ACP-AA and NP-ACP-OLA-AA), demonstrating that NPs improve the presence of the drug in the tumor, probably due to the EPR (enhanced permeability and retention) effect, making the treatment more effective and efficiently introduced into the tumor tissue.[46] Mesas et al demonstrated the accumulation of ACP nanoparticles functionalized with biologically active compounds from a natural extract (BC-ACP) in the colonic mucosa (alizarin red staining) but not in the liver or spleen (mono-nuclear phagocyte system).[34] This recent study suggested the prevention of BC-ACP sequestration in organs other than the tumor tissue, one of the great workhorses for the clinical application of nanoformulations. These nanoparticles (either ACP or Bc-ACP) were found to be hemocompatible and showed total absence of toxicity against white cells.[34] Calcium phosphate nanoparticles loaded with doxorubicin also exhibited enhanced tumor specificity in breast and pancreatic tumor models due to the prolonged stable circulation in the blood and an enhanced EPR effect.[47,48] These studies indicated that NPs showed excellent tumor accumulation with high specificity, which enhanced the bioavailability of the drug to tumors. Moreover, the protective effect of nanoparticles on AA further contributes to the improvement of therapeutic results, extending their time of action in synergy with OLA.

In addition, treatment of subcutaneous tumors with NP-ACP-OLA-AA resulted in a significant decrease of the expression of two markers of cellular malignancy, STAT3 and EGFR. The STAT3 gene is essential for tumor cell survival and regulation of the self-renewal capacity of tumor stem cells.[49] Meanwhile, EGFR expression is linked to several cancer-related signaling pathways, playing an important role in resistance to chemo- and radiotherapy, in the process of angiogenesis and in the regulation of cell apoptosis. In fact, EGFR is overexpressed in a significant percentage of pancreatic cancer patients, ranging from 30% to 89%.[50] The interaction between STAT3 and EGFR is necessary for tumor development, and Chen et al developed a molecule capable of inhibiting STAT3 and its interaction with EGFR, suppressing the progression of pancreatic cancer.[51] These findings underscore the potential of NP-ACP-OLA-AA as a promising therapeutic strategy for combating pancreatic cancer by reducing the expression of key genes involved in pancreatic cancer.

Among the great advantages of these biomimetic calcium phosphate nanoparticles are their exceptional biocompatibility and biodegradability. These nanoparticles exhibit remarkable similarities to bone and teeth, making them highly compatible with biological systems.[52] Calcium phosphate nanoparticles by themselves have no inherent toxicity but NPs can lead to an increase of the intracellular calcium concentration after endosomal uptake and lysosomal degradation.[53,54] Nonetheless, cells are able to clear the calcium from the cytoplasm in a short time. In fact, in vivo studies revealed that calcium phosphate nanoparticles inside the body do not pose risk since they are typically resorbed and dissolved by osteoclasts and macrophages.[53] The biocompatibility of calcium phosphate nanoparticles has also been demonstrated in vivo.[15] Mice injected with the different amounts of NPs were found to be alive and in good shape for at least 3 months, the latest time point checked. Moreover, the histological examination of sections of liver, spleen, kidney, and lung prepared from animals 3 days, 1 month and 3 months after NPs intravenous injection did not show signs of pathological conditions.[15]

Despite the reduced efficacy of the Olaparib-adsorbed NP (NP-ACP-OLA) in in vitro cytotoxicity studies, the dual surface functionalization of ACP NPs with OLA and AA has provided very interesting results in vitro and in vivo, being a very promising therapeutic strategy compared to other types of nanoformulations, as described before. It is worth mentioning that a clinical trial is ongoing (Phase II study, NCT05501548) to evaluate the safety and clinical activity of the combination of OLA and ascorbate in castration-resistant prostate cancer patients with no known DNA repair pathways. This study also opens the door for future clinical studies aimed at demonstrating the safety and clinical effectivity of dual nanosystem developed in this manuscript.

Conclusions

We have functionalized calcium phosphate NPs with OLA (75% loading efficiency and 13% payload) and AA (1% payload). Furthermore, the resulting dual nanosystem exhibited a controlled release of OLA together with protective effect of AA, improving the in vitro efficacy of the free drug in all cell lines tested, enhancing its ability to induce genotoxicity and apoptosis. This effect was confirmed using immunosuppressed in vivo models, which showed a greater inhibition of tumor growth compared to the free drug and better survival. Therefore, the NP-ACP-OLA-AA nanoformulation is postulated as a very promising candidate to improve the existing therapy against pancreatic cancer, enhancing the antitumor effect of the free OLA.

Acknowledgments

This work has been carried out in the framework of the projects RYC2021-032734-I and PDC2022-133191-I00 (nanoSOP) funded by Ministerio de Ciencia, Innovación y Universidades-Agencia Estatal de Investigación (MCIN/AEI/10.13039/501100011033) and the "European Union NextGenerationEU/PRTR", and project PMPTA22/00136 funded by the Instituto de Salud Carlos III (FEDER). Support from the University of Granada and the Spanish Ministry of Universities under the program "María Zambrano" is also acknowledged.

Disclosure

All authors report a patent P202331095 pending to University of Granada. The authors report no other conflicts of interest in this work.

References

1. Mizrahi JD, Surana R, Valle JW, Shroff RT. Pancreatic cancer. *Lancet*. 2020;395(10242):2008–2020. doi:10.1016/S0140-6736(20)30974-0
2. Mohammed S, Van Buren G, Fisher WE. Pancreatic cancer: advances in treatment. *World J Gastroenterol*. 2014;20(28):9354–9360. doi:10.3748/wjg.v20.i28.9354
3. Park W, Chawla A, O'Reilly EM. Pancreatic Cancer: a Review. *J Am Med Assoc*. 2021;326(9):851–862. doi:10.1001/jama.2021.13027
4. Faraoni I, Graziani G. Role of BRCA mutations in cancer treatment with poly(ADP-ribose) polymerase (PARP) inhibitors. *Cancers*. 2018;10(12):487. doi:10.3390/cancers10120487
5. Zhu H, Wei M, Xu J, et al. PARP inhibitors in pancreatic cancer: molecular mechanisms and clinical applications. *Mol Cancer*. 2020;34(9):987–1011. doi:10.1186/s12943-020-01167-9
6. Golan T, Hammel P, Reni M, et al. Maintenance Olaparib for germline BRCA-mutated metastatic pancreatic cancer. *N Engl J Med*. 2019;381(4):317–327. doi:10.1056/NEJMOA1903387
7. Mensah LB, Morton SW, Li J, et al. Layer-by-layer nanoparticles for novel delivery of cisplatin and PARP inhibitors for platinum-based drug resistance therapy in ovarian cancer. *Bioeng Transl Med*. 2019;4(2):e10131. doi:10.1002/BTM2.10131
8. Du C, Qi Y, Zhang Y, et al. Epidermal growth factor receptor-targeting peptide nanoparticles simultaneously deliver gemcitabine and olaparib to treat pancreatic cancer with breast cancer 2 (BRCA2) mutation. *ACS Nano*. 2018;12(11):10785–10796. doi:10.1021/acsnano.8b01573
9. Carvalho BG, Vit FF, Carvalho HF, Han SW, de la Torre LG. Recent advances in co-delivery nanosystems for synergistic action in cancer treatment. *J Mater Chem B*. 2021;9(5):1208–1237. doi:10.1039/D0TB02168G
10. Demiray M. Combinatorial therapy of high dose vitamin C and PARP inhibitors in DNA repair deficiency: a series of 8 patients. *Integr Cancer Ther*. 2020;19:1534735420969812. doi:10.1177/1534735420969812
11. Schoenfeld JD, Sibenaller ZA, Mapuskar KA, et al. O2·- and H2O2-mediated disruption of fe metabolism causes the differential susceptibility of NSCLC and GBM cancer cells to pharmacological ascorbate. *Cancer Cell*. 2017;31(4):487–500. doi:10.1016/j.ccell.2017.02.018
12. Mitchell MJ, Billingsley MM, Haley RM, Wechsler ME, Peppas NA, Langer R. Engineering precision nanoparticles for drug delivery. *Nat Rev Drug Discov*. 2020;20(2):101–124. doi:10.1038/s41573-020-0090-8
13. Wang W, Xiong Y, Hu X, et al. Codelivery of adavosertib and olaparib by tumor-targeting nanoparticles for augmented efficacy and reduced toxicity. *Acta Biomater*. 2023;157:428–441. doi:10.1016/j.actbio.2022.12.021
14. Gómez-Morales J, Iafisco M, Delgado-López JM, Sarda S, Drouet C. Progress on the preparation of nanocrystalline apatites and surface characterization: overview of fundamental and applied aspects. *Prog Cryst Growth Charact Mater*. 2013;59(1):1–46. doi:10.1016/j.pcrysgrow.2012.11.001
15. Oltolina F, Gregoletto L, Colangelo D, Gómez-Morales J, Delgado-López JM, Prat M. Monoclonal antibody-targeted fluorescein-5-isothiocyanate-labeled biomimetic nanoapatites: a promising fluorescent probe for imaging applications. *Langmuir*. 2015;31(5):1766–1775. doi:10.1021/la503747s
16. Khalifehzadeh R, Arami H. Biodegradable calcium phosphate nanoparticles for cancer therapy. *Adv Colloid Interface Sci*. 2020;279:102157. doi:10.1016/J.CIS.2020.102157
17. Guan Q, Zhou Le L, Lv FH, Li WY, Li YA, Dong Bin Y. A glycosylated covalent organic framework equipped with BODIPY and CaCO3 for synergistic tumor therapy. *Angew Chemie Int Ed*. 2020;59(41):18042–18047. doi:10.1002/anie.202008055
18. Chen J, Qiu M, Zhang S, et al. A calcium phosphate drug carrier loading with 5-fluorouracil achieving a synergistic effect for pancreatic cancer therapy. *J Colloid Interface Sci*. 2022;605:263–273. doi:10.1016/j.jcis.2021.07.080

19. Delgado-López JM, Iafisco M, Rodríguez I, Tampieri A, Prat M, Gómez-Morales J. Crystallization of bioinspired citrate-functionalized nanoapatite with tailored carbonate content. *Acta Biomater*. 2012;8(9):3491–3499. doi:10.1016/j.actbio.2012.04.046
20. Gallarate M, Carlotti ME, Trotta M, Bovo S. On the stability of ascorbic acid in emulsified systems for topical and cosmetic use. *Int J Pharm*. 1999;188(2):233–241. doi:10.1016/S0378-5173(99)00228-8
21. Grada A, Otero-Vinas M, Prieto-Castrillo F, Obagi Z, Falanga V. Research techniques made simple: analysis of collective cell migration using the wound healing assay. *J Invest Dermatol*. 2017;137(2):e11–e16. doi:10.1016/j.jid.2016.11.020
22. Thorsell A-G, Ekblad T, Karlberg T, et al. Structural basis for potency and promiscuity in poly(ADP-ribose) polymerase (PARP) and tankyrase inhibitors. *J Med Chem*. 2017;60(4):1262–1271. doi:10.1021/acs.jmedchem.6b00990
23. Rodríguez-Ruiz I, Delgado-López JM, Durán-Olivencia MA, et al. PH-responsive delivery of doxorubicin from citrate-apatite nanocrystals with tailored carbonate content. *Langmuir*. 2013;29(26):8213–8221. doi:10.1021/la4008334
24. Iafisco M, Ramírez-Rodríguez GB, Sakhno Y, et al. The growth mechanism of apatite nanocrystals assisted by citrate: relevance to bone biomineralization. *Cryst Eng Comm*. 2015;17(3):507–511. doi:10.1039/c4ce01415d
25. Yohannan Panicker C, Tresa Varghese H, Philip D. FT-IR, FT-Raman and SERS spectra of Vitamin C. *Spectrochim Acta*. 2006;65(3–4):802–804. doi:10.1016/j.saa.2005.12.044
26. Novo B, Bonanomi J, De Fiore S, Calogero F. Crystalline and amorphous forms of olaparib; 2017.
27. Delgado-López JM, Frison R, Cervellino A, Gómez-Morales J, Guagliardi A, Masciocchi N. Crystal size, morphology, and growth mechanism in bio-inspired apatite nanocrystals. *Adv Funct Mater*. 2014;24:1090–1099. doi:10.1002/adfm.201302075
28. Bruschi M. Mathematical models of drug release. In: *Strategies to Modify the Drug Release from Pharmaceutical Systems*. Elsevier; 2015:63–86. doi:10.1016/b978-0-08-100092-2.00005-9
29. Hu H, Zhang Y, Ji W, et al. Hyaluronic acid-coated and Olaparib-loaded PEI − PLGA nanoparticles for the targeted therapy of triple negative breast cancer. *J Microencapsul*. 2021;39(1):25–36. doi:10.1080/02652048.2021.2014586
30. Novohradsky V, Zajac J, Vrana O, Kasparkova J, Brabec V. Simultaneous delivery of olaparib and carboplatin in PEGylated liposomes imparts this drug combination hypersensitivity and selectivity for breast tumor cells. *Oncotarget*. 2018;9(47):28456–28473. doi:10.18632/oncotarget.25466
31. Caster JM, Sethi M, Kowalczyk S, et al. Nanoparticle delivery of chemosensitizers improve chemotherapy efficacy without incurring additional toxicity. *Nanoscale*. 2015;7(6):2805–2811. doi:10.1039/c4nr07102f
32. Van De Ven AL, Tangutoori S, Baldwin P, et al. Nanoformulation of olaparib amplifies PARP inhibition and sensitizes PTEN/TP53-deficient prostate cancer to radiation. *Mol Cancer Ther*. 2017;16(7):1279–1289. doi:10.1158/1535-7163.MCT-16-0740
33. Ma Y, Chen P, Drisko J, Khabele D, Godwin A, Chen Q. Pharmacological ascorbate induces 'BRCAness' and enhances the effects of Poly (ADP-Ribose) polymerase inhibitors against BRCA1/2 wild-type ovarian cancer. *Oncol Lett*. 2020;19(4):2629–2638. doi:10.3892/ol.2020.11364
34. Mesas C, Garcés V, Martínez R, et al. Colon cancer therapy with calcium phosphate nanoparticles loading bioactive compounds from Euphorbia lathyris: in vitro and in vivo assay. *Bio Pharmacr*. 2022;155:113723. doi:10.1016/j.biopha.2022.113723
35. Iafisco M, Delgado-Lopez JM, Varoni EM, et al. Cell surface receptor targeted biomimetic apatite nanocrystals for cancer therapy. *Small*. 2013;9 (22):3834–3844. doi:10.1002/smll.201202843
36. Buranasudja V, Doskey CM, Gibson AR, et al. Pharmacologic ascorbate primes pancreatic cancer cells for death by rewiring cellular energetics and inducing DNA damage. *Mol Cancer Res*. 2019;17(10):2102–2114. doi:10.1158/1541-7786.MCR-19-0381
37. Mao X, Du S, Yang Z, et al. Inhibitors of PARP-1 exert inhibitory effects on the biological characteristics of hepatocellular carcinoma cells in vitro. *Mol Med Rep*. 2017;16(1):208–214. doi:10.3892/MMR.2017.6568
38. Prasad CB, Prasad SB, Yadav SS, et al. Olaparib modulates DNA repair efficiency, sensitizes cervical cancer cells to cisplatin and exhibits anti-metastatic property. *Sci Rep*. 2017;7(1):1–15. doi:10.1038/s41598-017-13232-3
39. Quiñonero F, Mesas C, Muñoz-Gámez JA, et al. PARP1 inhibition by Olaparib reduces the lethality of pancreatic cancer cells and increases their sensitivity to Gemcitabine. *Bio Pharmacr*. 2022;155:113669. doi:10.1016/j.biopha.2022.113669
40. Roy I, McAllister DM, Gorse E, et al. Pancreatic cancer cell migration and metastasis is regulated by chemokine-biased agonism and bioenergetic signaling. *Cancer Res*. 2015;75(17):3529–3542. doi:10.1158/0008-5472.CAN-14-2645
41. Li D, Hu C, Yang J, et al. Enhanced anti-cancer effect of folate-conjugated olaparib nanoparticles combined with radiotherapy in cervical carcinoma. *Int J Nanomedicine*. 2020;15:10045–10058. doi:10.2147/IJN.S272730
42. Nakamura N, Fujihara H, Kawaguchi K, et al. Possible action of olaparib for preventing invasion of oral squamous cell carcinoma in vitro and in vivo. *Int J Mol Sci*. 2022;23(5):2527. doi:10.3390/ijms23052527
43. Wu M, Liu J, Hu C, et al. Olaparib nanoparticles potentiated radiosensitization effects on lung cancer. *Int J Nanomedicine*. 2018;13:8461–8472. doi:10.2147/IJN.S181546
44. Zhang Y, Hu H, Tang W, et al. A multifunctional magnetic nanosystem based on "two strikes" effect for synergistic anticancer therapy in triple-negative breast cancer. *J Control Release*. 2020;322:401–415. doi:10.1016/j.jconrel.2020.03.036
45. Rosenblum D, Joshi N, Tao W, Karp JM, Peer D. Progress and challenges towards targeted delivery of cancer therapeutics. *Nat Commun*. 2018;9 (1):1410. doi:10.1038/s41467-018-03705-y
46. Kalyane D, Raval N, Maheshwari R, Tambe V, Kalia K, Tekade RK. Employment of enhanced permeability and retention effect (EPR): nanoparticle-based precision tools for targeting of therapeutic and diagnostic agent in cancer. *Mater Sci Eng C*. 2019;98:1252–1276. doi:10.1016/j.msec.2019.01.066
47. Min KH, Lee HJ, Kim K, Kwon IC, Jeong SY, Lee SC. The tumor accumulation and therapeutic efficacy of doxorubicin carried in calcium phosphate-reinforced polymer nanoparticles. *Biomaterials*. 2012;33(23):5788–5797. doi:10.1016/j.biomaterials.2012.04.057
48. Kang Y, Sun W, Li S, et al. Oligo hyaluronan-coated silica/hydroxyapatite degradable nanoparticles for targeted cancer treatment. *Adv Sci*. 2019;6 (13):1900716. doi:10.1002/advs.201900716
49. Corcoran RB, Contino G, Deshpande V, et al. STAT3 plays a critical role in KRAS-induced pancreatic tumorigenesis. *Cancer Res*. 2011;71 (14):5020–5029. doi:10.1158/0008-5472.CAN-11-0908
50. Grapa CM, Mocan T, Gonciar D, et al. Epidermal growth factor receptor and its role in pancreatic cancer treatment mediated by nanoparticles. *Int J Nanomedicine*. 2019;14:9693–9706. doi:10.2147/IJN.S226628
51. Chen H, Bian A, Yang L, et al. Targeting STAT3 by a small molecule suppresses pancreatic cancer progression. *Oncogene*. 2021;40(8):1440–1457. doi:10.1038/s41388-020-01626-z

52. Sokolova V, Epple M. Biological and medical applications of calcium phosphate nanoparticles. *Chem Eur J*. 2021;27(27):7471–7488. doi:10.1002/chem.202005257
53. Epple M. Review of potential health risks associated with nanoscopic calcium phosphate. *Acta Bio*. 2018;77:1–14. doi:10.1016/j.actbio.2018.07.036
54. Sandhöfer B, Meckel M, Delgado-López JM, et al. Synthesis and preliminary in vivo evaluation of well-dispersed biomimetic nanocrystalline apatites labeled with positron emission tomographic imaging agents. *ACS Appl Mater Interfaces*. 2015;7(19):10623–10633. doi:10.1021/acsami.5b02624